Eur. Phys. J. A **24**, 223–229 (2005)
DOI 10.1140/epja/i2004-10138-1

THE EUROPEAN PHYSICAL JOURNAL A

Deformation and orientation effects in the driving potential of the dinuclear model

Qingfeng Li[1,7], Wei Zuo[2,3], Wenfei Li[2,3], Nan Wang[4], Enguang Zhao[1,2,5], Junqing Li[1,2,3,a], and W. Scheid[6]

[1] Institute of Theoretical Physics, Chinese Academy of Sciences, P.O. Box 2735, Beijing 100080, PRC
[2] Institute of Modern Physics, Chinese Academy of Sciences, Lanzhou 730000, PRC
[3] Research Center of Nuclear Theory of National Laboratory of Heavy Ion Accelerator of Lanzhou, Lanzhou 730000, PRC
[4] Department of Physics, College of Science, Shenzhen University, Shenzhen 518060 PRC
[5] Department of Physics, Tsinghua University, Beijing 100084, PRC
[6] Institut für Theoretische Physik, Justus-Liebig-Universität, D-35392, Giessen, Germany
[7] FIAS, Universität Frankfurt, D-60054, Frankfurt, Germany

Received: 13 August 2004 / Revised version: 17 January 2005 /
Published online: 18 March 2005 –
Communicated by A. Molinari

Abstract. A double-folding method is used to calculate the nuclear and Coulomb interaction between two deformed nuclei with arbitrary orientations. A simplified Skryme-type interaction is adopted. The contributions of the nuclear and Coulomb interactions due to the deformation and orientation of the nuclei are evaluated for the driving potential used in the description of heavy-ion fusion reaction. So far there is no satisfactory theory to describe the evolution of the dynamical nuclear deformation and orientations during the heavy-ion fusion process. Our results estimate the magnitude of the above effects.

PACS. 25.70.Jj Fusion and fusion-fission reactions – 25.70.-z Low and intermediate energy heavy-ion reactions – 24.10.-i Nuclear reaction models and methods

1 Introduction

The activity of the study on the synthesis of super-heavy elements is still hotly maintained both experimentally and theoretically. On the experimental branch, S. Hofmann and his collaborators [1] from GSI, Darmstadt, performed experiments on the synthesis and identification of the nuclei $^{272}111$ and $^{277}112$ in order to confirm their previous results obtained in the middle of the 1990s [2,3]. Furthermore, several additional decay chains from the reactions $^{64}\mathrm{Ni} + {}^{209}\mathrm{Bi} \rightarrow {}^{273}111^*$ and $^{70}\mathrm{Zn} + {}^{208}\mathrm{Pb} \rightarrow {}^{278}112^*$ were also measured. The joint IUPAC-IUPAP Working Party (IWP) has confirmed the discovery of the element with atomic number 110, which is named as darmstadtium (Ds); recently the new element with atomic number 111 has also been proposed by IWP to be named as roentgenium (Rg). Experiments on the synthesis of new elements with atomic numbers 115 as well as 113 in the reaction $^{243}\mathrm{Am} + {}^{48}\mathrm{Ca}$ were carried out at the U400 cyclotron in Dubna [4]; recently they also reported the results of excitation-function measurements for the $^{244}\mathrm{Pu} + {}^{48}\mathrm{Ca}$ fusion-evaporation reactions for element 114 and the synthesis of new isotopes of element 116 with the $^{245}\mathrm{Cm} + {}^{48}\mathrm{Ca}$ reaction [5].

On the theoretical branch, the physics on the more complicated dynamical process to super-heavy elements has been paid more attention to [6] and investigated by several groups under different mechanisms, for example, the dinuclear concept (see the recent works in [7–9] and the references therein), the fluctuation-dissipation model [10,11], the concept of nucleon collectivization [12, 13], as well as the macroscopic dynamical model [14,15].

In the dinuclear system (DNS) concept [7–9,16–19], the fusion process is considered as the evolution of a dinuclear system caused by the transfer of nucleons from the light nucleus to the heavy one. The nucleon transfer process is described in ref. [8] by solving the master equation numerically. It is found that the fusion probability of the compound nucleus is very sensitive to the specific form of the driving potential. In ref. [8], the Coulomb interaction potential of deformed nuclei with a tip-tip orientation is considered. However, spherical nuclei were adopted in calculating the nuclear interactions, and there the deformation effect is simulated by shifting the distance of nuclei to a smaller relative one determined by the same distance between the nuclear surfaces as the one that the deformed nuclei have. Although some reasonable results, such as the optimal excitation energies, the residual cross-sections of super-heavy compound nuclei, were obtained

[a] e-mail: jqli@impcas.ac.cn

for different heavy-ion fusion reactions, the reliability has to be checked.

Presently, a double-folding method is developed to calculate the nuclear and Coulomb interactions between the two deformed nuclei with arbitrary orientations. Here we consider the ground-state deformations of the nuclei for all possible combinations of the DNS of a certain reaction. In principle, the deformed nuclei can have different relative orientations which supply quite different conditions for fusion. Some averaging over the orientations of the nuclei has to be carried out at least in the entrance channel. The deformation and the orientation evolutions are difficult to be described, and have not yet been investigated very well by any model so far. Nevertheless, it is important to bear in mind what are the magnitudes that the deformation of nuclei contributes to the nuclear and Coulomb interactions, respectively, and to explore how and to which extent the orientations contribute. These investigations will give a direction for further improvement.

The paper is arranged as follows. In the next section, the treatment of the nuclear and Coulomb potentials is introduced. We present the calculated results and the corresponding discussions in sect. 3, where the interaction potentials between different deformed nuclei and their dependence on orientations as well as the driving potentials used in the DNS model for different fragmentations are presented for reactions leading to ^{272}Ds. Finally, sect. 4 gives a brief conclusion and outlook.

2 Treatment of driving potentials for orientated deformed nuclei of DNS

For a dinuclear system, the local excitation energy is defined as follows:

$$\epsilon^* = E^* - U(A_1, A_2, R) - \frac{(J-M)^2}{2\mathcal{J}_{\rm rel}} - \frac{M^2}{2\mathcal{J}_{\rm int}}, \qquad (1)$$

where E^* is the intrinsic excitation energy of the dinuclear system converted from the relative kinetic energy loss, M is the corresponding intrinsic spin due to the dissipation of relative angular momentum J. $\mathcal{J}_{\rm rel}$ and $\mathcal{J}_{\rm int}$ are the relative and intrinsic moments of inertia, respectively. $U(A_1, A_2)$ is the driving potential energy responsible for the nucleon transfer in the DNS model, and is written down as

$$\begin{aligned} U(A_1, A_2, R) = {} & U_{\rm LD+SC}(A_1) + U_{\rm LD+SC}(A_2) \\ & - U_{\rm LD+SC}(A_{\rm CN}) + U_{\rm C}(A_1, A_2, R) \\ & + U_{\rm N}(A_1, A_2, R), \end{aligned} \qquad (2)$$

where A_1, A_2, and $A_{\rm CN}$ represent the mass numbers of the two nuclei and the corresponding compound nucleus, respectively. We have $A_1 + A_2 = A_{\rm CN}$. In the DNS model, the driving potential is normally given as a function of $\eta = (A_1 - A_2)/A_{\rm CN}$. The first three parts on the right-hand side of the equation are calculated from the Liquid-Drop model plus the shell and pairing corrections [20,21]. $U_{\rm C}(A_1, A_2, R)$ and $U_{\rm N}(A_1, A_2, R)$ are the corresponding

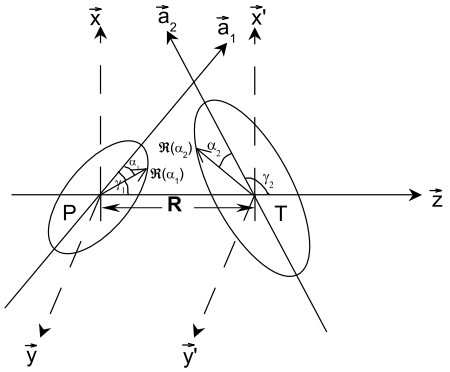

Fig. 1. Schematic presentation of the orientation of two deformed nuclei with axially symmetric quadrupole deformations.

Coulomb and nuclear potential energies between the nuclei and depend on the fragmentation of the dinuclear system, on the internuclear distance R and on the orientation and deformation of the nuclei. They could be calculated by different methods. In the present work, we calculate them by using the double-folding method:

$$U(\mathbf{r}_1 - \mathbf{r}_2) = \int \rho_1(\mathbf{r}_1)\rho_2(\mathbf{r}_2)\upsilon(\mathbf{r}_1 - \mathbf{r}_2 - \mathbf{R})\mathrm{d}\mathbf{r}_1\mathrm{d}\mathbf{r}_2, \quad (3)$$

where $\rho_1(\mathbf{r}_1)$ and $\rho_2(\mathbf{r}_2)$ are the density distribution of nucleus 1 and 2 in the dinuclear system, $\upsilon(\mathbf{r}_1 - \mathbf{r}_2 - \mathbf{R})$ is the corresponding interaction between the two points. For the nuclear part $U_{\rm N}$ we use densities with a smooth falling-off at the surface (see later) and constant densities for the Coulomb interaction. The long-range Coulomb interaction is not sensitive to the density at the surface which allows to simplify the calculations. Therefore, we write the Coulomb interaction as follows:

$$U_{\rm C}(R) = \rho_1^0\rho_2^0 \int \frac{\mathrm{d}\mathbf{r}_1\mathrm{d}\mathbf{r}_2}{|\mathbf{r}_1 - \mathbf{r}_2 - \mathbf{R}|}, \qquad (4)$$

where $\mathbf{R}$ is the vector between the two centers of the nuclei ("T" and "P") as illustrated in fig. 1. The charge densities are set as $\rho_1^0 = \frac{Z_1 e}{\Omega_1}$ and $\rho_2^0 = \frac{Z_2 e}{\Omega_2}$, where $Z_{1,2}$ and $\Omega_{1,2}$ are the proton numbers and the volumes of the two nuclei, respectively. The symmetry axes ($\vec{a}_1$ and $\vec{a}_2$) of the two deformed nuclei and the $\vec{z}$-axis are assumed to be in the same plane. γ_1 and γ_2 are the corresponding angles between the symmetric axes and the $\vec{z}$-axis, *i.e.*, which represent the different orientations of the two nuclei, while α_1 and α_2 are the angles between arbitrary vectors $\mathbf{r}_{1,2}$ and the symmetry axes $\vec{a}_1$ and $\vec{a}_2$, respectively. The distance between the two points is given by

$$|\mathbf{r}_1 - \mathbf{r}_2 - \mathbf{R}| = \sqrt{(\mathbf{r}_1 - \mathbf{r}_2)^2 + R^2 - 2(\mathbf{r}_1 - \mathbf{r}_2)\cdot\mathbf{R}}. \quad (5)$$

It is easy to find the following relations:

$$\begin{aligned} (\mathbf{r}_1 - \mathbf{r}_2)^2 = {} & r_1^2 + r_2^2 - 2r_1r_2(\sin\theta_1\sin\theta_2\cos(\phi_1 - \phi_2) \\ & + \cos\theta_1\cos\theta_2), \end{aligned} \qquad (6)$$

$$(\mathbf{r}_1 - \mathbf{r}_2)\cdot\mathbf{R} = (r_1\cos\theta_1 - r_2\cos\theta_2)R, \qquad (7)$$

where $\theta_{1,2}$ and $\phi_{1,2}$ are the angles of $\mathbf{r}_{1,2}$ with respect to the coordinates $(\vec{x}, \vec{y}, \vec{z})$ and $(\vec{x}\,', \vec{y}\,', \vec{z}\,')$, respectively.

The upper and lower limits of $r_{1,2}$, $\theta_{1,2}$, and $\phi_{1,2}$ are

$$r_{1,2} : (0, \Re(\alpha_{1,2})); \quad \theta_{1,2} : (0, \pi); \quad \phi_{1,2} : (0, 2\pi), \quad (8)$$

where $\Re(\alpha_1)$ and $\Re(\alpha_2)$ describe the nuclear surface with quadrupole deformations,

$$\Re(\alpha_i) = R_{0i}(1 + \beta_2^i Y_{20}(\alpha_i)). \quad (9)$$

Here R_{0i} are the spherical radii of the two nuclei which preserve their fixed volumes. $Y_{20}(\alpha) = (5/4\pi)^{1/2} P_2(\cos\alpha) = (5/4\pi)^{1/2}(3\cos^2\alpha - 1)/2$ is a spherical harmonics and the axial symmetry is preserved. The β_2^i is the quadrupole deformation parameter of the i-nucleus taken from ref. [21]. It is easy to write down the expressions for α_1 and α_2 as

$$\cos\alpha_1 = \hat{\vec{a}}_1 \cdot \hat{\Re}(\alpha_1) = \sin\theta_1 \cos\phi_1 \sin\gamma_1 + \cos\theta_1 \cos\gamma_1, \quad (10)$$

and

$$\cos\alpha_2 = \hat{\vec{a}}_2 \cdot \hat{\Re}(\alpha_2) = \sin\theta_2 \cos\phi_2 \sin\gamma_2 + \cos\theta_2 \cos\gamma_2. \quad (11)$$

For the nuclear potential, following the work by Adamian *et al.* [19], we adopt the Skyrme-type interaction without considering the momentum and spin dependence, in which a zero-range treatment of the effective interaction $\delta(\mathbf{r}_1 - \mathbf{r}_2)$ is assumed. The nuclear potential is obtained in the sudden approximation [19],

$$U_{\rm N}(R) = C_0 \Bigg\{ \frac{F_{\rm in} - F_{\rm ex}}{\rho_{00}} \Bigg(\int \rho_1^2(\mathbf{r}) \rho_2(\mathbf{r} - \mathbf{R}) {\rm d}\mathbf{r} + \int \rho_1(\mathbf{r}) \rho_2^2(\mathbf{r} - \mathbf{R}) {\rm d}\mathbf{r} \Bigg) + F_{\rm ex} \int \rho_1(\mathbf{r}) \rho_2(\mathbf{r} - \mathbf{R}) {\rm d}\mathbf{r} \Bigg\} \quad (12)$$

with

$$F_{\rm in,ex} = f_{\rm in,ex} + f'_{\rm in,ex} \frac{N_1 - Z_1}{A_1} \frac{N_2 - Z_2}{A_2}. \quad (13)$$

Here $N_{1,2}$ and $Z_{1,2}$ are the neutron and proton numbers of the two nuclei, respectively. Obviously, the isospin effect of the nucleon-nucleon interaction is considered here though the relative influence is small. The parameters $C_0 = 300\,{\rm MeV} \cdot {\rm fm}^3$, $f_{\rm in} = 0.09$, $f_{\rm ex} = -2.59$, $f'_{\rm in} = 0.42$, $f'_{\rm ex} = 0.54$, and $\rho_{00} = 0.17\,{\rm fm}^{-3}$ are also used in this work. The functions ρ_1 and ρ_2 are two-parameter Woods-Saxon density distributions (now we set the center of the P-nucleus at the coordinate origin and $\mathbf{r}_1 = \mathbf{r}$):

$$\rho_1(\mathbf{r}) = \frac{\rho_{00}}{1 + \exp((r - \Re_1(\alpha_1))/a_{\rho_1})} \quad (14)$$

and

$$\rho_2(\mathbf{r}) = \frac{\rho_{00}}{1 + \exp((|\mathbf{r} - \mathbf{R}| - \Re_2(\alpha_2))/a_{\rho_2})}. \quad (15)$$

The parameters a_{ρ_1} and a_{ρ_2} represent the diffuseness of the two nuclei, respectively. Whereas $\cos\alpha_1$ is given in eq. (10), we use the following formula with $|\mathbf{r} - \mathbf{R}| = \sqrt{r^2 + R^2 - 2rR\cos\theta}$:

$$\cos\alpha_2 = \frac{(\mathbf{r} - \mathbf{R}) \cdot \hat{\vec{a}}_2}{|\mathbf{r} - \mathbf{R}|} = \frac{r(\sin\theta\cos\phi\sin\gamma_2 + \cos\theta\cos\gamma_2) - R\cos\gamma_2}{r^2 + R^2 - 2rR\cos\theta}. \quad (16)$$

We directly calculate the six- and three-dimensional integrals in eqs. (4) and (12) numerically. For eq. (12), a truncation parameter $r_{\rm cut}$ for the upper limit of r is introduced due to the long tails of the nuclear densities expressed in eqs. (14) and (15). For each mass asymmetry we calculated the sum of the Coulomb and nuclear potential energies as a function of the internuclear distance R and took the potential at the minimum in R which is shorter than $R_{\rm CB}$ (Coulomb-barrier saddle point).

3 Numerical results

In the present paper, the nuclear and Coulomb interaction for the DNS of the reaction $^{64}{\rm Ni} + {}^{208}{\rm Pb} \to {}^{272}{\rm Ds}$ is studied by taking the nuclear deformations and the corresponding orientations into account. For simplicity, the diffuseness parameters a_{ρ_1} and a_{ρ_2} are chosen as $a_{\rho_1} = a_{\rho_2} = 0.6$ fm, which is a little bit larger than those in ref. [19]. Furthermore, $r_{01} = r_{02} = 1.2$ fm is used. The parameter $r_{\rm cut} = 25$ fm for the radial integration of the nuclear potential of the deformed nucleus in eq. (12), is taken for an adequate precision.

Figures 2(a) and (b) show the nuclear interaction potentials of two sets of projectile-target combinations, namely $^{28}{\rm Na} + {}^{244}{\rm Es}$ and $^{74}{\rm Zn} + {}^{198}{\rm Hg}$, to form the same compound nucleus $^{272}{\rm Ds}$ as a function of distance R between the centers of the two nuclei. The corresponding nucleus-nucleus potentials including both the nuclear and Coulomb interactions are given in figs. 2(c) and (d). In figs. 2(a) and (c), both nuclei are with prolate deformation, $^{28}{\rm Na}$ with $\beta_2 = 0.257$ and $^{244}{\rm Es}$ with $\beta_2 = 0.234$, respectively, while in figs. 2(b) and (d), $^{74}{\rm Zn}$ is prolate and $^{198}{\rm Hg}$ oblate with $\beta_2 = 0.125$ and -0.112, respectively. The system $^{74}{\rm Zn} + {}^{198}{\rm Hg}$ is more mass-symmetric, *i.e.*, it has a smaller $|\eta|$ than the system $^{28}{\rm Na} + {}^{244}{\rm Es}$, and thus a higher Coulomb potential energy. In each panel, different orientations for the two systems, *i.e.*, tip-tip, tip-belly and belly-belly orientations are investigated, an illustration is shown in the (c) plot. When both β_2 values are positive in (a) and (c), the angles $(\gamma_1, \gamma_2) = (0°, 180°)$, $(0°, 90°)$, and $(90°, 90°)$ are the corresponding ones for the tip-tip, tip-belly, and belly-belly cases, respectively, while for the case of $\beta_2^1 > 0$ and $\beta_2^2 < 0$ in cases (b) and (d), $(\gamma_1, \gamma_2) = (0°, 90°)$, $(0°, 0°)$, and $(90°, 0°)$, are corresponding to the tip-tip, tip-belly, and belly-belly cases, respectively. The two nuclei become more compact with a belly-belly orientation in contrast to the tip-tip one, *i.e.* the minimum of the potential energy for a belly-belly orientation is at a smaller R than that of the tip-tip case.

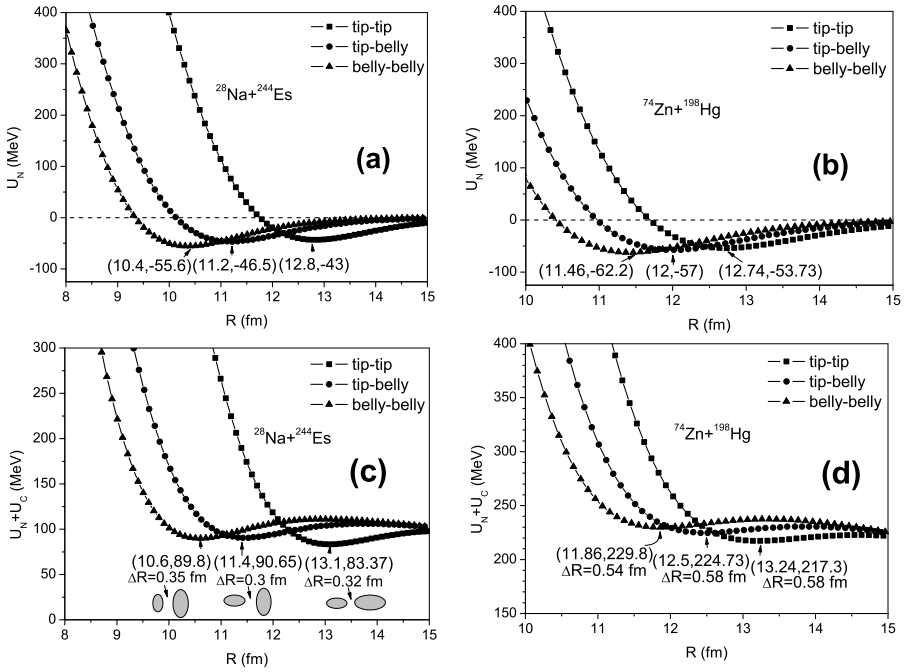

Fig. 2. The nuclear (in (a) and (b)) and the nuclear+Coulomb potentials (in (c) and (d)) for two sets of projectile-target combinations for the same compound nucleus ^{272}Ds are shown as a function of R for different orientations of the two nuclei.

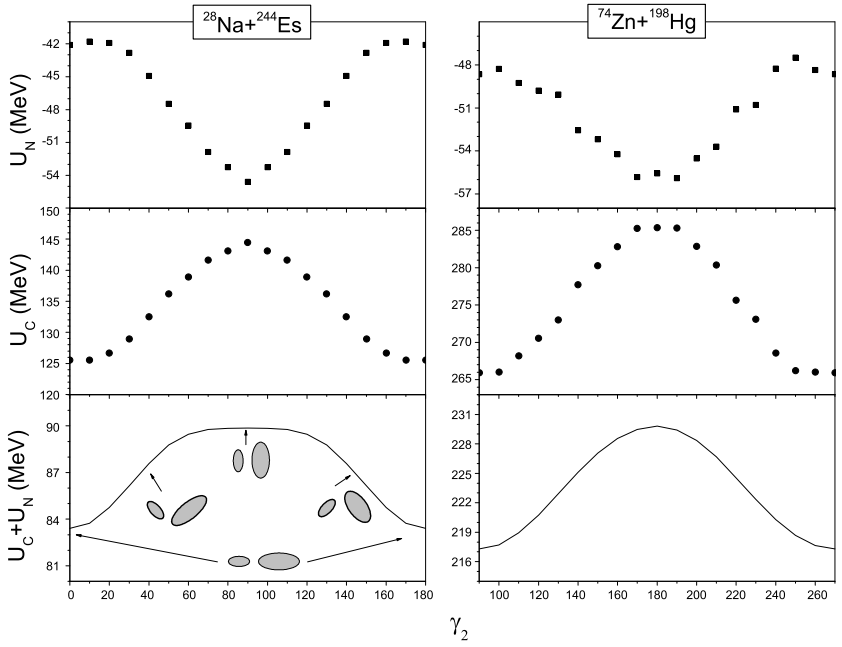

Fig. 3. The potentials with $\gamma_1 + \gamma_2 = 180^\circ$ for ^{28}Na + ^{244}Es (left panel) and $\gamma_1 + \gamma_2 = 90^\circ$ for ^{74}Zn + ^{198}Hg (right panel). See the text for details.

The depth of the potential pocket is higher for the belly-belly case which is in favor of the fusion for entrance channel. However, for the intermediate channel during the nucleon transfer, the tip-tip orientation seems preferable, since the minimum potential energy is lower. When the orientation changes from the tip-tip type to the belly-belly one, the minima of the nuclear potentials in (a) and (b) behave differently as those of the total potentials shown in (c) and (d), *i.e.*, the minima of the nuclear interaction go down while the minima of the total interaction increase. The reason for the decrease from tip-belly to belly-belly in (c) is that the increase of the Coulomb interaction energy is smaller than the decrease of the nuclear interaction energy. Defining a distance between the surface of the two nuclei, for example, for the tip-tip case, $\Delta R = R_{\min} - (\Re_1^{\text{long}} + \Re_2^{\text{long}})$, while for the belly-belly

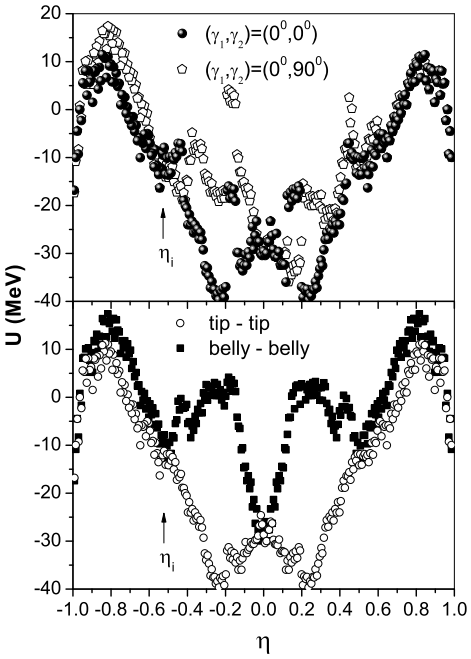

Fig. 4. The driving potentials with different orientations for the system ^{272}Ds. The calculation was started with the ^{64}Ni + ^{208}Pb fragmentation (see the text).

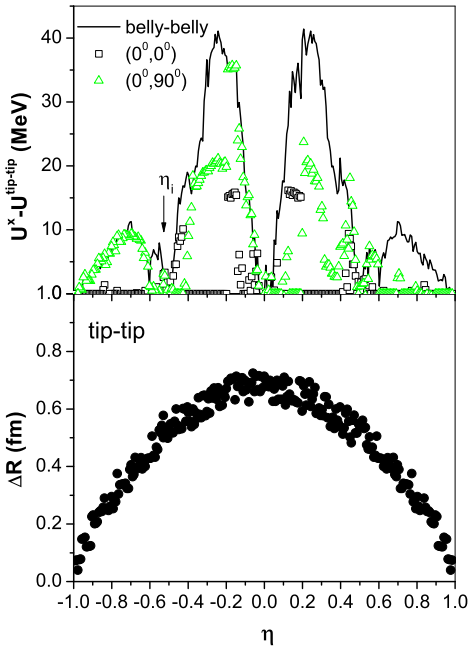

Fig. 5. Top: the difference between the driving potentials of tip-tip case and the other cases. Bottom: ΔR as a function of η with tip-tip orientation for the same reaction system as in fig. 4.

case, $\Delta R = R_{\rm min} - (\Re_1^{\rm short} + \Re_2^{\rm short})$ ($\Re_i^{\rm long,short}$ represent the long and short axes of the deformed nucleus i, respectively), we find that ΔR changes a little for different orientations. When $|\eta|$ decreases from 1 to 0, the value of ΔR increases due to a larger repulsive Coulomb force. Therefore, the effect of the mass asymmetry and the orientation of the DNS on the driving potential can be analyzed from these results.

Figure 3 shows the potentials at the minimum of $U_{\rm N} + U_{\rm C}$ illustrated in fig. 2 for the above two combinations as a function of the orientation, the orientation is chosen in a way that keeps $\gamma_1 + \gamma_2 = 180°$ for the system ^{28}Na + ^{244}Es and $\gamma_1 + \gamma_2 = 90°$ for ^{74}Zn + ^{198}Hg. On the left-hand side, γ_1 goes from 180° to 0° and γ_2 from 0° to 180°; on the right-hand side, γ_1 is chosen from 0° to −180° and γ_2 from 90° to 270° in order to obtain similar trends of the variation of potentials as a function of the orientation of the two nuclei as on the left-hand side. In the two cases, both of the orientations change from the tip-tip orientation to the belly-belly one and finally back to the tip-tip orientation (the orientation of the nuclei is shown in the lower-left plot of fig. 3). With the changing of the orientations of the two nuclei, the nuclear potentials (upper panels) form a valley while the Coulomb potentials (middle panels) attain a peak value for the tip-tip orientation. The summation of the two contributions shown in the bottom panels is similar in shape to the Coulomb potential but the change with angle is gentler.

Figure 4 displays the driving potentials in eq. (2) for different orientations. In the upper panel of the figure we fixed γ_1 and γ_2 to 0° or 90°, while in the lower panel, the results for the tip-tip and belly-belly orientations are shown. The points in fig. 4 were calculated by starting with the initial fragmentation ^{64}Ni + ^{208}Pb (η_i) transferring nucleons in steps of one proton or one neutron by searching for the minimum of potential energy. Therefore, the potentials are only approximately symmetric with respect to $\eta = 0$ for the tip-tip and belly-belly cases, while for the cases with orientations of $(0°, 0°)$ and $(0°, 90°)$ in the upper panel, this symmetry is lost obviously. From fig. 4, we find that the driving potential is quite sensitive to the choice of the orientation of the two nuclei. The driving potential for the tip-tip configuration is smaller than that for the belly-belly configuration in the whole range of η. This result is different from that obtained in ref. [22], and might be associated to another consideration of the fusion process of heavy ions.

To evaluate the difference between the different orientations, we show the differences between the potential energies of the various cases with respect to the tip-tip case in the upper half of fig. 5, where $U^{\rm belly\text{-}belly} - U^{\rm tip\text{-}tip}$ is shown with a line, while the other two cases are shown with different scattered symbols. The differences are peaked in two regions, one in $|\eta| < 0.5$ and the other in $|\eta| > 0.5$. In each region there exists a large deformation of the nuclei, especially when $|\eta|$ is $0.1 \sim 0.4$. However, the detailed deformation of the two nuclei in each part is different, that is, when $|\eta| > 0.5$, the smaller nucleus is almost spherical while the larger counterpart is prolately deformed. When $|\eta| < 0.5$, prolate and oblate deformations of the two nuclei occur, for example, for $\eta = -0.243$, the corresponding configuration is ^{103}Mo + ^{169}Er with a couple of large prolate deformation $(\beta_2^1, \beta_2^2) = (0.358, 0.304)$. When $\eta = -0.169$, the corresponding ^{113}Pd + ^{159}Gd consists of a negatively (−0.25) deformed ^{113}Pd and a

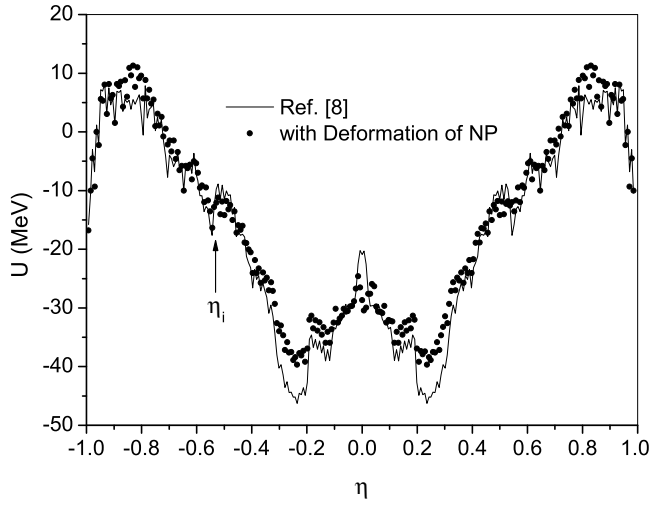

Fig. 6. The comparison of the driving potential by using the ground-state deformation and the tip-tip orientation for both the nuclear and Coulomb interactions with previous calculations of ref. [8] (see the text) for the system $^{64}\mathrm{Ni} + {}^{208}\mathrm{Pb} \rightarrow {}^{272}\mathrm{Ds}$.

positively (0.28) deformed ^{159}Gd. The separation distance ΔR between the surfaces of the two nuclei of the DNS is shown in the lower graph of fig. 5. Because of the relatively large Coulomb potential, ΔR is stretched when the masses of the two participating nuclei become more equal, which has also been shown in fig. 2.

For the dinuclear system $^{64}\mathrm{Ni} + {}^{208}\mathrm{Pb} \rightarrow {}^{272}\mathrm{Ds}$, fig. 6 shows the comparison between the present driving potential shown by dots and that calculated in a way as being used in ref. [8] shown by a fine line for the tip-tip orientation. In the present calculations, the ground-state deformation has been taken into account for both the nuclear and Coulomb interactions. In ref. [8], a parameterized Morse formula [16] has been adopted for the nuclear part of the potential with nuclei assumed as spherical but shifted to a smaller relative distance determined by the same distance between the nuclear surfaces as the one which the deformed nuclei have. In this manner the deformation of the nuclei was simulated in the nuclear part of the potential of ref. [8]. Here, for the sake of convenience the diffuseness parameters are taken as $a_{\rho_1} = a_{\rho_2} = 0.6$ fm for the present calculation and $a_1 = a_2 = 0.6$ fm for the parameterized Morse formula. We find that the two potentials are basically very close to each other; however, some obvious deviations appear in the relatively large deformed regions, for example, around $|\eta| \sim 0.2$ and $|\eta| \sim 0.8$. It should be pointed out that a deviation also occurs at $|\eta| \sim 0$. After checking the detailed path of evolution, we find that the configurations of the DNS in the two cases are different at this point. For the case with a nuclear interaction of spherical nuclei, the combination ($^{136}\mathrm{La} + {}^{136}\mathrm{I}$) is preferred, while for the one with that of deformed nuclei, a more charge-symmetric combination ($^{136}\mathrm{Ba} + {}^{136}\mathrm{Xe}$) is taken into account. Obviously, the effect of a large deformation in the deformed region $|\eta| \sim 0.2$ changes the final path of the evolution near $\eta = 0$. In the region with larger deformation, the results from ref. [8] is lower than our calculated ones shown by dots. The reason is that the nucleus-nucleus interaction has been overestimated by the method of ref. [8]. The present calculation clarified the overestimation.

4 Conclusion and outlook

A double-folding method used to calculate the nucleus-nucleus potential between deformed nuclei is further developed to improve the driving potential of nuclear fusion in the DNS model. By taking into account the nuclear deformation in the nuclear interaction together with the Coulomb interaction, the formalism for calculating the driving potential of heavy-ion fusion becomes more reasonable. The deformations and orientations of the interacting nuclei contributing to the nuclear and Coulomb interactions are investigated for every fragmentation of the DNS considered. It is natural that the tip-tip orientation has the lowest interaction energy, and may be preferred during the nucleon exchange process. The minimum energies of the nucleus-nucleus interaction along the distance between the centers of the two nuclei appear at larger distances when the mass-asymmetry $|\eta|$ changes from unit to zero, which is due to the larger Coulomb force, and is in favor for the quasi-fission process. So far, a dynamical evolution of the deformation and orientation during the heavy-ion fusion process is not reasonably treated by the present models to our knowledge. Our results have estimated the effects of the deformation and orientation of the nuclei, on the driving potential. Hopefully they will give a direction for a further investigation and improvement.

In a future study, we will calculate the fusion probability of various projectile-target combinations with deformed nuclei. Furthermore, when the distance between the surfaces of the two nuclei is elongated the effect of quasi-fission is expected more pronounced. We will further consider a two-dimensional potential as a function of the mass asymmetry η and the internuclear distance R in order to investigate the effect of quasi-fission in a subsequent work.

The authors (Q. Li, W. Zuo, E. Zhao, J. Li, and W. Li) acknowledge the warm hospitality of the Insitut für Theoretische Physik, Universität Giessen, Germany. They are also grateful to Dr A. Diaz- Torres for valuable discussions. The work is supported by: the National Natural Science Foundation of China under Grants 10175082, 10235020, 10375001, 10311130175; the Major Basic Research Development Program under Grant No. G2000-0774-07; the Knowledge Innovation Project of the Chinese Academy of Sciences under Grant No. KJCX2-SW-N02; One Hundred Person Project of CSA; K.C. Wong Post-doctors Research Award Fund of CAS; the Alexander von Humboldt Foundation; the National key program for Basic Research of the Ministry of Science and Technology (2001CCB01200, 2002CCB00200); the Natural Science Foundation of Guangdong province under Grant 04300874 and the financial support from DFG of Germany.

References

1. S. Hofmann *et al.*, Eur. Phys. J. A **14**, 147 (2002).
2. S. Hofmann *et al.*, Z. Phys. A **350**, 277 (1995).
3. S. Hofmann *et al.*, Z. Phys. A **354**, 229 (1996).
4. Yu.Ts. Oganessian *et al.*, Phys. Rev. C **69**, 021601R (2004); **69**, 029902E (2004)(E).
5. Yu.Ts. Oganessian *et al.*, Phys. Rev. C **69**, 054607 (2004).
6. A.C. Berriman, D.J. Hinde, M. Dasgupta, C.R. Morton, R.D. Butt, J.O. Newton, Nature **413**, 144 (2001).
7. G.G. Adamian, N.V. Antonenko, W. Scheid, Phys. Rev. C **69** 011601R; 014607 (2004).
8. W.F. Li, N. Wang, J.F. Li, H.S. Xu, W. Zuo, E.G. Zhao, J.Q. Li, W. Scheid, Europhys. Lett. **64**, 750 (2003).
9. G. Fazio, G. Giardina, A. Lamberto, R. Ruggeri, C. Sacca, R. Palamara, A.I. Muminov, A.K. Nasirov, U.T. Yakhshiev, F. Hanappe, T. Materna, L. Stuttge, Eur. Phys. J. A **19**, 89 (2004).
10. C.W. Shen, G. Kosenko, Y. Abe, Phys. Rev. C **66**, 061602 (2002).
11. Y. Abe, B. Bouriquet, Nucl. Phys. A **722**, 241 (2003); **733**, 321 (2004)(E).
12. V.I. Zagrebaev, Phys. Rev. C **64**, 034606 (2001).
13. V.I. Zagrebaev, Nucl. Phys. A **734**, 164 (2004).
14. W.J. Swiatecki, Phys. Scr. **24**, 113 (1981).
15. J.P. Blocki, H. Feldmeier, W.J. Swiatecki, Nucl. Phys. A **459**, 145 (1986).
16. G.G. Adamian, N.V. Antonenko, W. Scheid, Nucl. Phys. A **618**, 176 (1997).
17. V.V. Volkov, Izv. Akad. Nauk SSSR, Ser. Fiz. **50**, 1879 (1986).
18. N.V. Antonenko, E.A. Cherepanov, A.K. Nasirov, V.B. Permjakov, V.V. Volkov, Phys. Lett. B **319**, 425 (1993).
19. G.G. Adamian, N.V. Antonenko, R.V. Jolos, S.P. Ivanova, O.I.Melnikova, Int. J. Mod. Phys. E **5**, 191 (1996).
20. W.D. Myers, W.J. Swiatecki, LBNL Report, UCRL-11980 (1965).
21. P. Möller, J.R. Nix, W.D. Myers, W.J. Swiatecki, At. Data Nucl. Data Tables **59**, 185 (1995).
22. Ş. Mişicu, W. Greiner, Phys. Rev. C **66**, 044606 (2002).